



## Hybrid acrylic nanocomposites with excellent transparency and hardness/toughness balance

Dušica B. Stojanović<sup>a,\*</sup>, Ljiljana Brajović<sup>b</sup>, Vera Obradović<sup>c</sup>, Daniel Mijailović<sup>c</sup>, Dragan Dramlić<sup>d</sup>, Aleksandar Kojić<sup>a</sup>, Petar S. Uskoković<sup>a</sup>

<sup>a</sup> University of Belgrade, Faculty of Technology and Metallurgy, Karnegijeva 4, 11120 Belgrade, Serbia

<sup>b</sup> University of Belgrade, Faculty of Civil Engineering, BulevarKralja Aleksandra 73/1, 11120 Belgrade, Serbia

<sup>c</sup> University of Belgrade, Innovation Center, Faculty of Technology and Metallurgy, Karnegijeva 4, 11120 Belgrade, Serbia

<sup>d</sup> University of Belgrade, Institute of Physics, Center for Experimental Physics, Pregevica 118, 11120 Belgrade, Serbia

### ARTICLE INFO

#### Keywords:

Composite nanofibers  
Hybrid acrylic films  
Mechanical and optical properties  
Mie scattering model

### ABSTRACT

The composite nanofibers were used as reinforcement in acrylic polymer for the overall enhancement of thermo-mechanical properties, adhesion between fibers and matrix, and fracture toughness of the final nanocomposite since acrylic materials lack of this feature. So, a good balance between hardness/toughness and transparency is obtained with the addition of poly (vinyl butyral) (PVB) and titania (TiO<sub>2</sub>) nanofibers simultaneously and controlling their contents. Specifically, when compared to that of pure acrylic polymer, the fracture toughness of the PMMA nanocomposite apparently increased 55 % with the addition of 3 wt.% titania nanoparticles, while the produced nanocomposite maintained high transmittance above 75–80% in the visible domain. The transmission spectrum modelling of the reinforced fiber materials and hybrid acrylic composites using Mie scattering theory for different particle sizes and particle content is presented. The calculated transmission coefficients versus wavelength are compared with the experimental ones.

### 1. Introduction

Poly (methyl methacrylate) (PMMA) is an important thermoplastic material with excellent transparency, and it has been widely used in optical and porous materials, biomedical materials, dental and surgical applications, and electronics. However, brittleness limits its applications. Many studies have been extensively carried out in order to enhance the physical and mechanical properties of PMMA, since the polymer-polymer composite is a promising approach, which incorporates polymer fibers into the PMMA polymer matrix to provide the toughening mechanisms for the composite. The fibers can redistribute the stress load on the composite and the small inter-fiber distance can stop crack propagation in the composite [1–3].

In recent years, electrospun nanofibers have attracted interest as reinforcements for composite materials due to their small diameter (20 nm–500 nm) and high aspect ratio. Nanocomposite fibers designate a new class of materials where the polymeric nanofibers are reinforced by dispersing inorganic fillers and nanofillers as well. Furthermore, electrospinning has the next facilities: (a) the diameters of fibrous materials are lessened to the nanometer scale dimensions; (b) produced nanofibrous mats possess a large surface area to mass ratio for

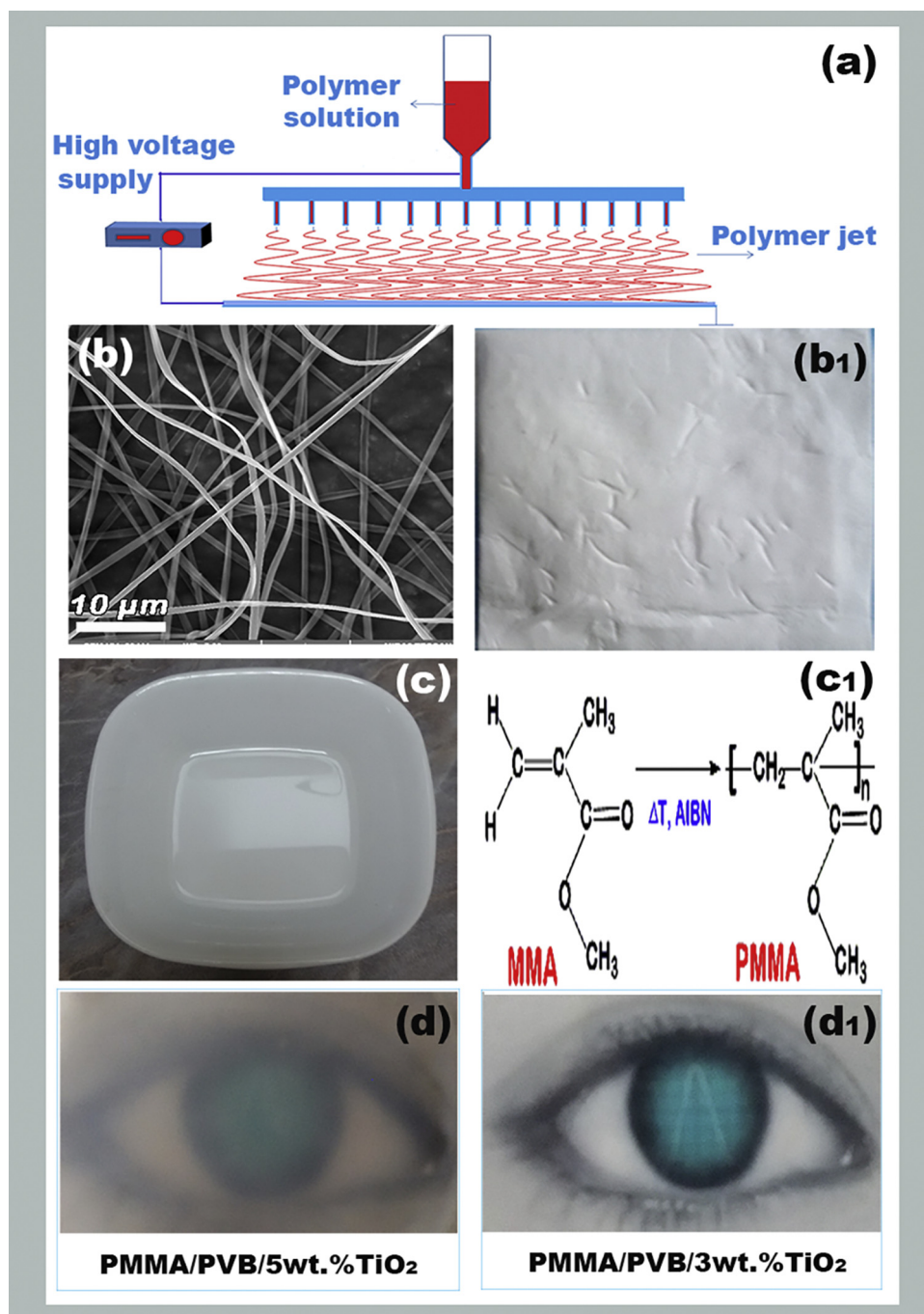
their better bonding which makes great mechanical strength of the matrix material; (c) nanoparticles can be dispersed in the spin solution and (d) the chemical stability of the nanoparticles during spinning and composite fabrication is not endangered [4].

So far, very few studies have reported the mechanical properties for electrospun composite nanofibers that are ideal candidates as reinforcement fillers [5]. In another study, it was demonstrated that a significant enhancement in tensile mechanical properties (tensile strength, Young's modulus and fracture toughness) of the novel PMMA nanocomposite with electrospun graphene-incorporated-Nylon 6 (Gr/PA-6) nanofibers as the reinforcement was achieved with a 0.01 wt.% Gr addition. In the visible wavelength range of 400–800 nm the maintained transmittance of the nanocomposite was above 70 % compared to the neat PMMA. For example, aligned Nylon 6 (PA-6) electrospun nanofibers were applied to reinforce the transparent PMMA polymer. In a similar approach, Yu et al. demonstrated completely transparent composites of PMMA filled with poly (vinyl butyral) nanofibers with perfectly matched refractive indices of matrix and filler (Table S1, see Supplementary data).

The results of the previous study approved the mechanical improvement of the PVB/TiO<sub>2</sub> electrospun mats since they had higher

\* Corresponding author.

E-mail address: [duca@tmf.bg.ac.rs](mailto:duca@tmf.bg.ac.rs) (D.B. Stojanović).



**Scheme 1.** Presentation of the preparation of transparent nanocomposite films in simplified steps.

values of the indentation hardness and reduced modulus compared to the neat PVB mats. Besides these properties, PVB/TiO<sub>2</sub> electrospun composite mats demonstrated satisfied antibacterial activity toward Gram-negative bacterium *Escherichia coli* [6]. In this study, the PVB/TiO<sub>2</sub> nanofibers were embedded into PMMA/MMA/AIBN solution to fabricate reinforced composite films by simply in-situ polymerization/cast technique (Scheme 1 and Fig. S1, Supplementary data). The mechanical and optical properties of PMMA composite films were steadily improved with 20 wt. % PVB/TiO<sub>2</sub> nanofiber content.

Mie and Rayleigh scattering theories for spherical particles can be used for modeling and calculating the optical transmittance of certain nanocomposites. Mie scattering theory exhibits the solution for the electromagnetic scattering by a sphere of radius *R* inserted in a surrounding homogeneous and isotropic medium which is illuminated by a

plane wave. The scattering cross section calculations for non-spherical shape particles are much more difficult than those coming from Mie theory for spherical ones. In this study, the transmittance coefficient dependence of the PVB/TiO<sub>2</sub> electrospun mats and acrylic nanocomposites on wavelength range has been evaluated by Mie scattering theory and compared with the experimental values (Fig. S2, Supplementary data).

The prepared transparent nanocomposites with excellent hardness/toughness balance can be applied as laminated safety glass in the automotive and aerospace industry. Due to the well-known antimicrobial properties of these materials, they can also be used for denture base applications.

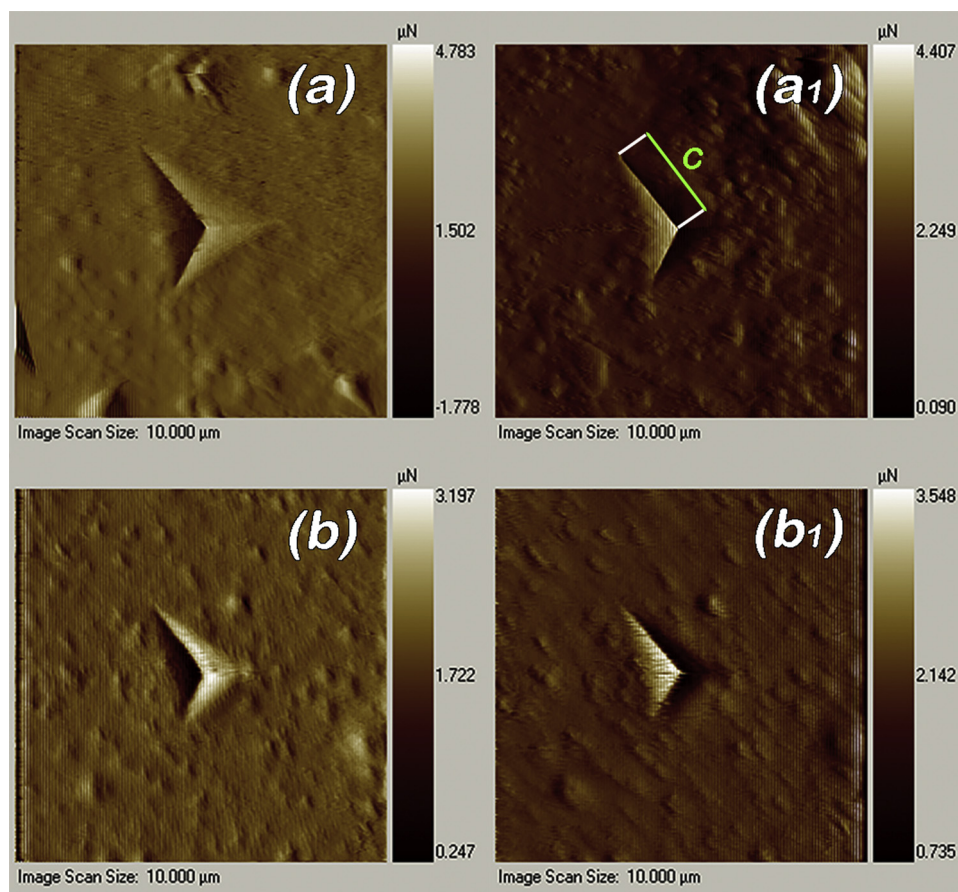


Fig. 1. Gradient in-situ SPM images (scan size of  $10 \times 10 \mu\text{m}$ ) of (a) neat PMMA and (b) PMMA/PVB/TiO<sub>2</sub> nanocomposites.

## 2. Materials and methods

### 2.1. Materials

PVB (Mowital B75H, Kuraray,  $M_w = 95,000\text{--}110,000 \text{ g/mol}$ ,  $n = 1.488$ ) is a resin usually used for applications that require strong binding, optical clarity, adhesion to many surfaces, toughness and flexibility. Commercially available PMMA Acryrex® CM205 (Chi Mei Corp., Taiwan, ( $M_w = 90,400 \text{ g/mol}$ ,  $n = 1.491$ )) pellets, liquid monomer (methyl methacrylate, (MMA)) and 2,2'-azobisisobutyronitrile (AIBN initiator was recrystallized from methanol) (Sigma Aldrich) were used for preparing samples. Commercial TiO<sub>2</sub> powder (Aeroxide P25) with a mean diameter of 21 nm was obtained from Evonik-Degussa, Germany.

### 2.2. Composite fabrication by in-situ polymerization/cast technique

The experiments were carried out with the PVB solution in a concentration of 8 wt.% where acetic acid/ethanol (20/80 wt./wt.) was used as the solvent for production neat and composite nanofibers. In this work, the electrospinning device used for the experiments was Electrospinner CH-01 (Linari Engineering, Italy). The multi-needle system (14 needles) was used in the experiments where the applied voltage was  $V = 28 \text{ kV}$  and the complete flow rate was  $Q = 7 \text{ ml/h}$ . The electrospun nanofibers were collected on an alkaline-resistant fiberglass mesh and dried in air for 15 h (Scheme 1a, b and b<sub>1</sub>) [6]. Then several layers of PVB mats were cut into  $10 \text{ cm} \times 10 \text{ cm}$  pieces and compacted in a hydraulic press at room temperature. The PMMA resin was prepared by mixing PMMA polymer in MMA monomer. The resulting solution was 10 wt.% PMMA in the MMA monomer. A polymerization initiator, AIBN, was added to the solution at a concentration of 2.5 mg/

ml (Scheme 1c<sub>1</sub>) [7].

The neat PVB mat and PVB mat reinforced with TiO<sub>2</sub> nanoparticles (20 wt.%) were soaked in the PMMA/MMA/AIBN solution for 5 h in the polystyrene mold (Scheme 1c), followed by drying in a vacuum oven at room temperature for 20 min. The PMMA resin containing the PVB mats was dried thoroughly in an oven at 65 °C for 12 h, and finally formed a transparent film (Scheme 1d and d<sub>1</sub>) at the bottom of the polystyrene mold, which was peeled off for characterization.

## 3. Characterization

The morphologies of the electrospun nanofibers and nanoparticles diameter distribution were investigated by transmission electron microscopy (TEM (JEOL 100CX II instrument)) at 100 kV. The mechanical properties of neat PMMA and PMMA composite film were tested using a Hysitron TI 950 TriboIndenter equipped with in-situ SPM (scanning probe microscopy) imaging and optical microscope (Hysitron, MN). A Berkovich indenter was used, and the indentation hardness, reduced elastic modulus and fracture toughness were calculated and recorded from nine different testing points. The analysis of nanoindentation data was performed using the Oliver and Pharr method [8], assuming a value of 0.45 for the Poisson's ratio. The indentation maximum load was set at 2000 μN for each tested sample. The loading and unloading times, as well as the hold time at the peak force, were all set to 25 s. The DMA measurements were performed on a dynamic mechanical analyzer (Q 800, TA Instruments) with a tensile mode at a frequency of 1 Hz. The scanning temperature range was from 30 °C to 110 °C at a scanning rate of 3 °C min<sup>-1</sup>. The sample size was  $25 \times 8 \times 1 \text{ mm}$ . Optical transmission spectra of the various kinds of prepared composites and pure polymer as control were measured in VIS and IR ranges using DU 720 General purpose UV-VIS spectrometer in the wavelength range from 200 to

**Table 1**  
Results of the roughness analysis for all the tested samples.

Samples	RMS (nm)	R <sub>p</sub> (nm)	R <sub>v</sub> (nm)
PMMA	14.55 (7.52)	186.93 (39.52)	84.24 (18.72)
PMMA/PVB/3 wt.% TiO <sub>2</sub>	15.53 (13.54)	125.33 (20.23)	67.25 (15.02)
PMMA/PVB/5 wt.% TiO <sub>2</sub>	27.28 (26.51)	173.73 (16.74)	76.10 (16.71)

1100 nm.

## 4. Results and discussion

### 4.1. Mechanical considerations

The frequently used method proposed by Oliver and Pharr [8], involves the extrapolation of a tangent to the top of the unloading curve to determine the depth (a combination of elastic and plastic displacement) over which the indenter is in contact with the specimen at the maximum load, P<sub>max</sub>. Indentation hardness is defined as the applied load per unit area of indentation (Fig. S3, Supplementary data). The fracture toughness can be calculated from the indentation hardness, the reduced elastic modulus, and the length of the crack size after nanoindentation (Equations S1-S5, Supplementary data and Fig. 1) [9]. The roughness values of the samples were measured using in-situ SPM imaging and the roughness analysis was performed by TriboView analysis software. The surface roughness can be characterized by some statistical parameters: the root mean square roughness (RMS), the maximum valley depth (R<sub>v</sub>) and the maximum peak height (R<sub>p</sub>), as listed in Table 1.

The addition of the nanoparticles increases the RMS of the nanocomposites surface and the typical root mean square roughness values for all the tested samples were 14.55 (7.52) nm, 15.53 (13.54) nm and 27.28 (26.51) nm, respectively, as shown in Fig. 1.

The resulting PMMA/PVB/TiO<sub>2</sub> composite containing 3 wt.% nanoparticles showed an increase in hardness by 35 % and elastic modulus by 60 % relative to neat PMMA, as determined using the nanoindentation technique. The results in Table 2 indicate that PMMA/PVB/TiO<sub>2</sub> composite containing 3 wt.% and 5 wt.% nanoparticles have a significantly higher fracture toughness compared with the neat polymer (2.73 (0.128) MPa m<sup>1/2</sup>, 4.24 (0.154) MPa m<sup>1/2</sup> and 3.16 (0.495) MPa m<sup>1/2</sup>, respectively). With the addition of 3 wt.% TiO<sub>2</sub> nanoparticles used as reinforcement, the hardness and modulus values are higher, indicating that the applied electrospinning procedure is suitable for the nanoparticle dispersion.

The addition of the PVB composite fibers into the PMMA matrix gradually increased the storage modulus compared to the neat PMMA sample. The modulus was more increased by the introduction of the PVB fibers which contained 3 wt.% TiO<sub>2</sub> nanoparticles due to their good dispersion in the electrospun PVB fibers. The highest value of the storage modulus at 30 °C was achieved for the PMMA/PVB/3 wt.% TiO<sub>2</sub> sample (1974 MPa) and the improvement was around 15 % compared to the neat PMMA sample (1719 MPa). Because PMMA is immiscible with PVB, two phases (Fig. S4, Supplementary data) and relaxation peaks corresponding to the individual T<sub>g</sub>s of PVB/TiO<sub>2</sub> and PMMA are detected in the Tan Delta curve for PMMA/PVB (80/20 wt./wt.) [10,11]. The peak with the highest transition temperature T<sub>g2</sub> is

**Table 2**

Nanomechanical properties of neat PMMA and PMMA/PVB/TiO<sub>2</sub> nanocomposites.

Samples	H (GPa)	E <sub>r</sub> (GPa)	K <sub>c</sub> (MPa m <sup>1/2</sup> )
PMMA	4.27 (0.060)	0.229 (0.208)	2.73 (0.128)
PMMA/PVB/3 wt.% TiO <sub>2</sub>	5.76 (0.188)	0.366 (0.343)	4.24 (0.154)
PMMA/PVB/5 wt.% TiO <sub>2</sub>	5.05 (0.676)	0.284 (0.717)	3.16 (0.495)

associated with the glass transition of a PMMA rich phase, and the lower transition temperature is attributed to the T<sub>g1</sub> of a PVB/TiO<sub>2</sub>-rich phase (Table 3).

The same relationship is with the loss factor, tan δ<sub>1</sub> and tan δ<sub>2</sub>. Tan δ<sub>2</sub> of the PMMA/PVB/3 wt.% TiO<sub>2</sub> sample had a lower value (0.913) and higher T<sub>g2</sub> (94.1 °C) compared to the neat PMMA sample (88.3 °C). For the sample with 3 wt.% TiO<sub>2</sub> nanoparticles the T<sub>g1</sub> and T<sub>g2</sub> were the highest, while the tan δ<sub>1</sub> and tan δ<sub>2</sub> had the lowest value compared to PMMA and PMMA/PVB/5 wt.% TiO<sub>2</sub> samples.

The temperature dependence of the storage modulus and loss factor (Tan Delta) for the PMMA samples is depicted in Fig. 2.

From Tan Delta values, adhesion factor A can be calculated, which is a parameter that indicates the presence of some interfacial interactions between the composite fibers and the matrix [12]. These results demonstrated that the 3 wt.% addition of the TiO<sub>2</sub> nanoparticles and their good dispersion in the PVB fibers, improved adhesion of the acrylic nanocomposites (Table 3 and Equation S5 (Supplementary data)).

The results for the adhesion efficiency and storage modulus from the DMA analysis were in coherence with the results for the hardness/toughness and reduced elastic modulus from the nanoindentation.

### 4.2. Optical considerations

The optical transmission of polymer composite films depends on scattering and absorption of light by the particles, as well as, absorption of light in the pure polymer matrix itself. The amount of scattered and absorbed energy on the single particle related to the incident radiation is expressed in terms of scattering and absorption cross sections. The materials used both as a matrix or reinforcement for the described polymer composites in this research were non-absorbing. The scattering cross section of particles should be calculated [13].

The scattering cross section σ<sub>s</sub> is defined as a ratio of scattered radiation power, P<sub>s</sub>, on the particle and radiation flux density F<sub>in</sub> incident on it [14]:

$$\sigma_s = \frac{P_s}{F_{in}} \quad (1)$$

One way to calculate the scattering cross section is to use Mie scattering theory that gives the solution in a case of scattering of the incident plane electromagnetic wave by a spherical particle of radius r, inserted in a surrounding homogeneous and isotropic medium. If the index of refraction of a particle material is n<sub>p</sub>, of a medium is n<sub>m</sub>, and the electromagnetic radiation wavelength in a vacuum is λ<sub>0</sub>, the scattering cross section depends on size parameter given as χ = 2·π·r·n<sub>m</sub>/λ<sub>0</sub>, and the ratio of refraction indices of particle and medium given as m = n<sub>p</sub>/n<sub>m</sub>. The size parameter compares the dimension of a particle and medium wavelength [15]. The calculations based on Mie theory are complicated and derive scattering cross section as an infinitive sum of parameters, which are obtained using special, (Bessel) function of χ and m. Nowadays, there is a great deal of the developed software for calculation of scattering and extinction cross sections. The values for the particular composite can be obtained using Mie scattering calculator shareware software [16].

If the size parameter is χ < < 1 (in practice χ < 0.2), the Mie calculated solutions can be approximated with Rayleigh scattering model values. Rayleigh scattering cross section is given by Eq. (2):

$$\sigma_s = \frac{128 \cdot \pi^6}{3} \cdot \left( \frac{m^2 - 1}{m^2 + 2} \right) \cdot \frac{r^6}{\lambda^4} \quad (2)$$

where r = d/2 represents a particle radius [14].

In order to calculate the scattering cross sections and transmission for the composites fabricated in this work, particle and agglomerates diameters in the range from 20 – 140 nm were used, (see Fig. 3(b, d)) as well as, indices of refraction for particle and matrix materials for the wavelengths in the range of 450 – 1100 nm. Since the size parameter criteria can be fulfilled for Rayleigh scattering for some wavelength and

**Table 3**  
DMA results for the PMMA composite samples.

Samples	E' (30 °C, MPa)	T <sub>g1</sub> (°C)	tan δ <sub>1</sub>	T <sub>g2</sub> (°C)	tan δ <sub>2</sub>	A (at tan δ <sub>max</sub> )
PMMA	1719	/	/	88.3	0.979	/
PMMA/PVB/3 wt.% TiO <sub>2</sub>	1974	87.9	0.883	94.1	0.913	0.187
PMMA/PVB/5 wt.% TiO <sub>2</sub>	1868	87.8	0.937	93.9	0.957	0.241

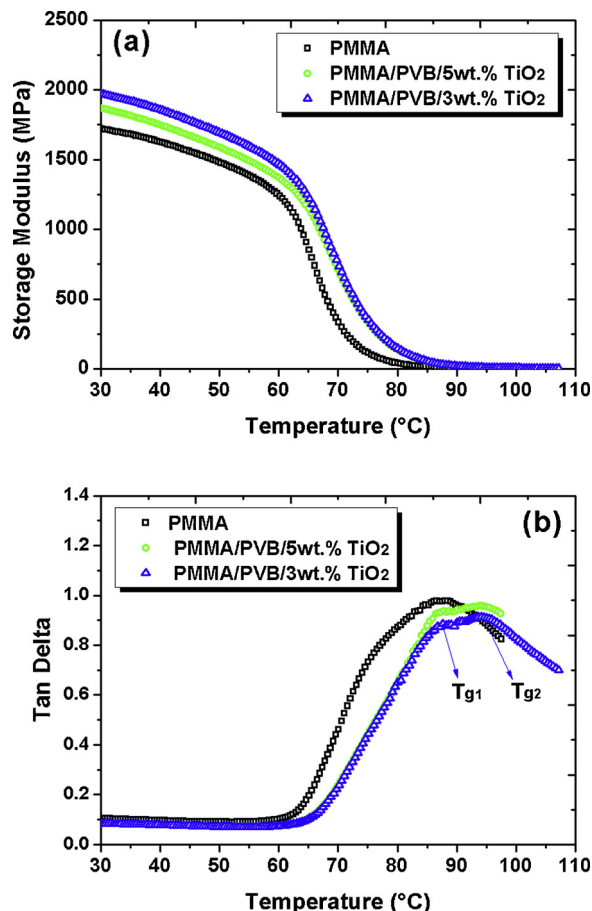


**Fig. 2.** Storage modulus and Tan Delta versus temperature curve for all the PMMA samples.

diameter ranges, the initial calculations were done using both Mie and Rayleigh scattering models. The differences up to 10 % in the obtained scattering cross sections were observed, especially for larger diameter particles. So, Rayleigh modeling, as much simpler, should be used for less accurate calculations, but the calculations presented in this paper are based on Mie scattering model. If two parallel planes, at distance  $L$ , are considered inside a polymer composite and if  $I_0$  is the intensity of incoming light at first plane and  $I$  is the intensity of transmitted light reaching the second plane, the transmission coefficient  $T$  can be calculated as [13]:

$$T = \frac{I}{I_0} = e^{-\gamma_S \cdot L} \quad (3)$$

where  $\gamma_S$  is a scattering coefficient of a polymer composite.

In the following text, the scattering cross section calculated using Mie theory is denoted as  $\sigma_{SM}$ . If particles in a composite are spherical with diameter  $d$ , their concentration number in a polymer is  $n_d$ , and their scattering cross section at a wavelength  $\lambda_0$  is  $\sigma_{SM}$ , the scattering coefficient of the polymer composite sample at that wavelength  $\gamma_S$  can be obtained as:

$$\gamma_S = n_d \cdot \sigma_{SM} \quad (4)$$

The total volume of all particles in the composite is denoted as  $V_p$  and it is connected with composite volume  $V_{comp}$  as:

$$V_p = f_v \cdot V_{comp} \quad (5)$$

where  $f_v$  is a total volume fraction of particles. Since the volume of one spherical particle of diameter  $d$  is:

$$V_d = \pi \cdot \frac{d^3}{6} \quad (6)$$

The total particle volume is:

$$V_p = N_d \cdot V_d = N_d \cdot \pi \cdot \frac{d^3}{6} = f_v \cdot V_{comp} \quad (7)$$

and number concentration is:

$$n_d = \frac{N_d}{V_{comp}} = \frac{f_v \cdot 6}{\pi \cdot d^3} \quad (8)$$

The transmission coefficient  $T$  in Eq. (3) is normalized to the transmission of the pure polymer sample of the same width and for the same wavelength. In order to calculate the transmission spectra of a sample normalized to the air, calculated transmission  $T$  should be multiplied with the transmission coefficients of the pure polymer film.

The calculations were done using Mie calculator software [16] for spherical particles and the concentration was given in  $1/\mu\text{m}^3$  unit. Input data for the calculations were: the mass density of PMMA  $\rho_{PMMA} = 1.18 \text{ g/cm}^3$ , the mass density of PVB  $\rho_{PVB} = 1.075 \text{ g/cm}^3$  and the mass density of TiO<sub>2</sub>  $\rho_{TiO_2} = 3.915 \text{ g/cm}^3$ . Based on those data the total volume fraction  $f_v$  of TiO<sub>2</sub> in composite samples is calculated using Eq. (9) [13]:

$$f_v = \frac{\rho_{pol} \cdot f_w}{(1 - f_w) \cdot \rho_{Ti} + \rho_{pol} \cdot f_w} \quad (9)$$

where  $f_w$  represents the total mass fraction of particles in the polymer composite,  $\rho_{pol}$  is a mass concentration of a polymer matrix. The values of  $f_w$  for the polymer composite were 3 wt.% or 5 wt.%. The indices of refraction values for used materials were taken from the manufacturer. Transmission for four different samples is calculated and compared with the measured ones. Sample No.1 had PVB electrospun mat and 3 wt.% of TiO<sub>2</sub> particles. Sample No.2 had the same particles and PVB mat, but the mass fraction of particles was 5 wt.%. Sample No.3 was made from PVB nanofibers mat with 3 wt.% of TiO<sub>2</sub> particles in the pure PMMA matrix. The sample No. 4 was made from similar nanofibers mat, but the mass fraction of TiO<sub>2</sub> in the nanofibers was 5 wt.%. The nanofibers mat mass fraction in a composite was 20 wt.%.

The scattering cross sections  $\sigma_{SM}$  were calculated for spherical particles of various diameters  $d$ , taken in the range 20 nm–140 nm at 10 nm steps, and for the wavelength range from 450 nm to 1100 nm in 50 nm steps. This range of diameters was chosen based on transmission electron microscopy images (Fig. 3(a, c)).

The nominal value of the nanoparticle diameter was 21 nm and the calculations were done for this diameter, too. For each sample, the volume of the overall particle is known based on  $f_w$ , and an idealistic situation was supposed, that all TiO<sub>2</sub> nanoparticles in the composite are spherical and have the same diameter.

Then for sample No.1 with 3 wt.% of particles, the  $f_v$  was calculated using Eq. (9) and based on this value the number concentrations  $n_d$  using Eq. (8) was obtained. Taking into account that the thickness of all

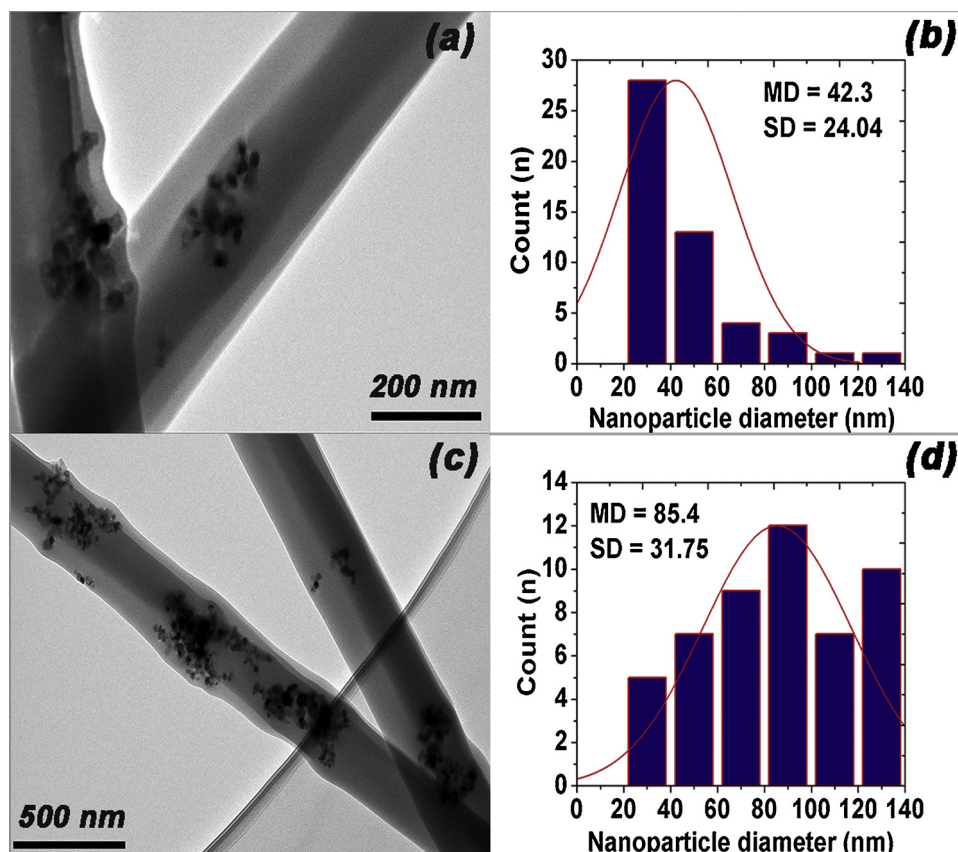


Fig. 3. Transmission electron microscopy images composite fibers (a, c) and nanoparticles size distribution (b, d).

the composite films was  $L = 1$  mm, the transmission coefficients were calculated for different diameters versus wavelength using Eq. (3). Thus calculated values represent the transmission coefficient versus pure polymer transmission.

Graphs displayed in Fig. 4a represent the dependence of calculated transmission coefficients of sample No.1 versus wavelength, for the different diameters of the embedded particles. As a comparison, the measured transmission of the sample No.1 is presented at the same graph as a solid line.

Comparing calculated curves in Fig. 4a, it is clearly visible that for every wavelength there is a maximum diameter which enables the transmission coefficient at least 5 % or greater. For example, for 450 nm wavelength particle diameter should be smaller than 30 nm and for 600 nm smaller than 70 nm. Also from the graph in Fig. 4a, it is obvious that when the particle diameter is some value above, the transmission coefficient at all wavelengths in the range is below 5 % and in Fig. 4a that diameter is 100 nm.

The measured transmission coefficients at different wavelengths match calculated values for different diameters, and that means that there is a distribution of particle diameter in the real composite that enables it to have transmission greater than 5 % in some wavelength range. The rough comparison of the measured and calculated results based on transmission spectra match on different diameters shows that the range of particle diameters that mostly influence the transmission of sample No.1 is from 20 to 90 nm.

In Fig. 4b the similar results are presented for sample No.2. Transmissions were generally smaller because of the larger mass fraction of particles and transmission is negligible up to 600 nm. The comparison of the measured and calculated values roughly shows that particles influence the transmission is in the range from 30 nm to 90 nm.

The mass fraction of  $\text{TiO}_2$  was  $f_W = 3$  wt.% or  $f_W = 5$  wt.% in fibers, while the mass fraction of the fibers was 20 wt.% in the polymer

composites with PMMA matrix. Thus, the real mass fraction of the  $\text{TiO}_2$  particles was 0.6 wt.% or 1 wt.% in the polymer composite samples No.3 and No.4 respectively. Since in this composite the  $\text{TiO}_2$  particles are in two polymers with different mass density and the same indices of refraction, for a total volume fraction  $f_V$  Eq. (10) is used.

$$f_V = \frac{\frac{0.2 \cdot f_W}{\rho_{\text{Ti}}} + \frac{(1 - f_W) \cdot 0.2}{\rho_{\text{PVB}}} + \frac{0.8}{\rho_{\text{PMMA}}}}{\frac{0.2 \cdot f_W}{\rho_{\text{Ti}}} + \frac{(1 - f_W) \cdot 0.2}{\rho_{\text{PVB}}} + \frac{0.8}{\rho_{\text{PMMA}}}} \quad (10)$$

In Fig. 5a, the graphs represent calculated transmission values for different diameters of the particles for the sample No.3, and the measured transmission coefficients a solid line. In this case, it was obvious that the smaller diameter particles had a greater influence on transmission and their roughly estimated range was from 20 to 40 nm and the particles with a diameter near 20 nm were dominant.

In Fig. 5b the similar graphs for sample No.4 are presented. The calculated and measured transmission coefficients were smaller than the ones of sample No.3, as expected. The estimated particle diameter range based on the comparison of measured and calculated transmission coefficients was from 20 to 60 nm, but particles around 30 nm are more dominant since the transmission at lower wavelengths is significantly smaller compared to sample No.3. Comparing the measured transmission coefficients for all four samples with the calculated transmission for the nominal  $d = 21$  nm shows that the dispersion in the sample No.3 is close to the ideal since shows measured and calculated transmission has an excellent match.

For used polymers  $\rho_{\text{PMMA}} \approx \rho_{\text{PVB}}$  i.e. there is a refractive index matching and the scattering on embedded nanofibers tends to be zero and the polymer phases are totally transparent [17]. So, in our case, the loss of transparency in the visible domain is attributed to the scattering of light by particles only. Analyzing the Mie scattering theory for different sizes of the particles, it can be concluded that the particles in the

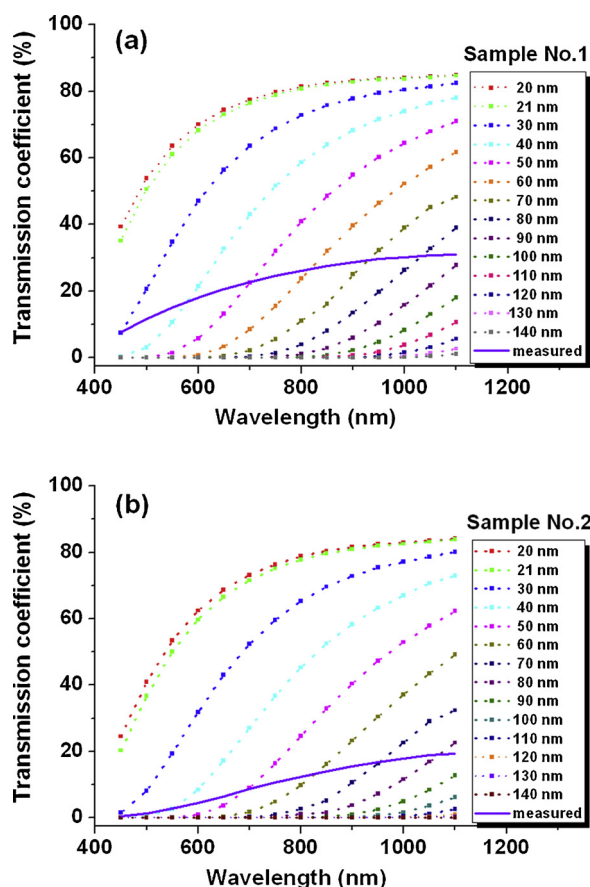


Fig. 4. Transmission coefficients normalized to the air vs. wavelength for samples No.1 and No.2.

composites from nanofibers have better dispersion and smaller agglomerates.

## 5. Conclusion

In summary, we investigated simply in-situ polymerization/cast techniques for the manufacture of functional electrospun nanofiber composites with optimized mechanical and optical properties. These processing methods are effective for achieving a good dispersion of nanofillers, adhesion and coherent nanofiber-matrix interfaces, with further functionality demonstrated for optically transparent electrospun nanofiber composites. The addition of PVB/TiO<sub>2</sub> nanofibers into the acrylic matrix clearly showed improvement in indentation hardness and fracture toughness properties. The optical transmission spectra modeling and measurements showed a better dispersion of particles in nanofibers composites. Also, this kind of composites can keep the high optical transmission in the visible range of  $450 \text{ nm} < \lambda < 800 \text{ nm}$ , with an appropriate mass fraction of TiO<sub>2</sub> particles in polymer nanofibers. The nanocomposite films manufactured using this technology have excellent transparency and hardness/toughness balance, making them very useful as coatings in various fields such as aerospace and automotive industries, healthcare, defense and security.

## Declaration of Competing Interest

The authors declare that they have no known competing financial interests or personal relationships that could have appeared to influence the work reported in this paper.

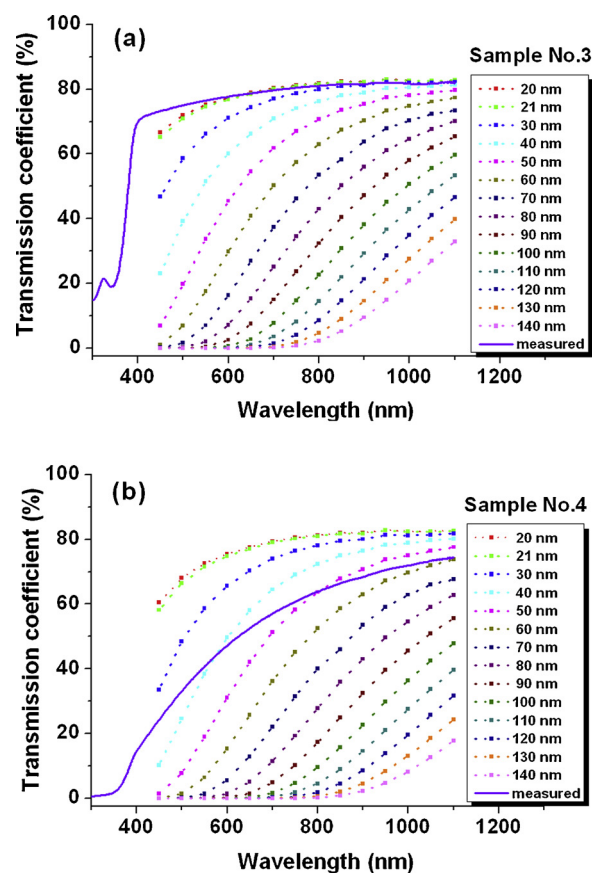


Fig. 5. Transmission coefficients normalized to the air vs. wavelength for samples No.3 and No.4.

## Acknowledgment

The authors acknowledge the support of the Ministry of Science, Technological Development and Education of Republic of Serbia for the support of this research through the projects TR 34011, III 45019 and III 45003.

## Appendix A. Supplementary data

Supplementary material related to this article can be found, in the online version, at doi:<https://doi.org/10.1016/j.porgcoat.2019.105437>.

## References

- [1] H. He, S. Chen, J. Bai, H. Zheng, B. Wu, M. Ma, Y. Shi, X. Wang, High transparency and toughness PMMA nanocomposites toughened by self-assembled 3D loofah-like gel networks: fabrication, mechanism, and insight into the in situ polymerization process, *RSC Adv.* 6 (2016) 34685–34691, <https://doi.org/10.1039/c6ra02723g>.
- [2] J.L.H. Chau, C.-C. Hsieh, Y.-M. Lin, A.-K. Li, Preparation of transparent silica-PMMA nanocomposite hard coatings, *Prog. Org. Coat.* 62 (2008) 436–439, <https://doi.org/10.1016/j.porgcoat.2008.02.005>.
- [3] F.A. Alzarrug, Synthesis and Characterization of Dental Composite Materials Reinforced With Nanofibers, PhD Thesis Faculty of Technology and Metallurgy, Belgrade, 2018, p. 102 <https://fedorabg.bg.ac.rs/fedora/get/o:19765/bdef:Content/get>.
- [4] S.A. Ben Hassan, D.B. Stojanovic, A. Kojovic, I.A. Castvan, D. Janackovic, P.S. Uskokovic, R. Aleksic, Preparation and characterization of poly (vinylbutyral) electrospun nanocomposite fibers reinforced with ultrasonically functionalized sepiolite, *Ceram. Int.* 40 (2014) 1139–1146, <https://doi.org/10.1016/j.ceramint.2013.06.115>.
- [5] S. Jiang, Y. Chen, G. Duan, C. Mei, A. Greiner, S. Agarwal, Electrospun nanofiber reinforced composites: a review, *Polym. Chem.* 9 (2018) 2685–2720, <https://doi.org/10.1039/C8PY00378E>.
- [6] F.A. Alzarrug, D.B. Stojanovic, V. Obradovic, A. Kojovic, M. Rajilic-Stojanovic, P.S. Uskokovic, Multiscale characterization of antimicrobial poly (vinyl butyral)/

- titaniananofibrous composites, *Polym. Adv. Technol.* 28 (2017) 909–914, <https://doi.org/10.1002/pat.3996>.
- [7] J.H. Yu, A.J. Hsieh, G.C. Rutledge, Novel Transparent PMMA Composites for Optical Tagging U. S. Army Research Laboratory, ARL-TR-5354, 2010, pp. 1–10 (Accessed May 9, 2019), <https://apps.dtic.mil/dtic/tr/fulltext/u2/a531405.pdf>.
- [8] W.C. Oliver, G.M. Pharr, Measurement of hardness and elastic modulus by instrumented indentation: advances in understanding and refinements to methodology, *J. Mater. Res.* 19 (2004) 3–20, <https://doi.org/10.1557/jmr.2004.19.1.3>.
- [9] D.B. Stojanovic, A. Orlovic, M. Zrilic, I. Balac, C.Y. Tang, P.S. Uskokovic, R. Aleksic, The effects of functionalization on the thermal and tribo-mechanical behaviors of neat and grafted polyethylene nanocomposites, *Polym. Compos.* 34 (2013) 1710–1719, <https://doi.org/10.1002/pc.22574>.
- [10] W. Chen, D.J. David, W.J. Mac Knight, F.E. Karasz, Miscibility and phase behavior in blends of poly (vinyl butyral) and poly (methyl methacrylate), *Macromolecules* 34 (2001) 4277–4284, <https://doi.org/10.1021/ma010072q>.
- [11] A.T. Almeida, H. Gliemann, Th. Schimmel, D.F.S. Petri, Characterization of PMMA/PVB blend films by means of AFM, *Microsc. Microanal.* 11 (2005) 122–125, <https://doi.org/10.1017/S1431927605051044>.
- [12] A.A. Naim, A.M.A. Elbary, S.S. Ibrahim, Dynamic mechanical analysis and non-isothermal kinetics of EVA/PPy carbon black nanocomposites, *Mater. Sci. Technol.* 35 (2019) 560–570, <https://doi.org/10.1080/02670836.2019.1572319>.
- [13] L.M. Brajovic, D.B. Stojanovic, P. Mihailovic, S.B. Markovic, M. Romcevic, M. Mitric, V. Lazovic, D. Dramlic, S. Petricevic, N. Romcevic, Preparation and characterization of bismuth germanium oxide (BGO) polymer composites, *J. Alloys Compd.* 695 (2017) 841–849, <https://doi.org/10.1016/j.jallcom.2016.10.140>.
- [14] W.G. Rees, Scattering systems, *Physical Principles of Remote Sensing*, Cambridge University Press, New York, 2012, pp. 281–317, <https://doi.org/10.1017/CBO9781139017411>.
- [15] D.B. Stojanovic, L.M. Brajovic, A. Orlovic, D. Dramlic, V. Radmilovic, P.S. Uskokovic, R. Aleksic, Transparent PMMA/silica nanocomposites containing silica nanoparticles coating under supercritical conditions, *Prog. Org. Coat.* 76 (2013) 626–631, <https://doi.org/10.1016/j.porgcoat.2012.12.002>.
- [16] Mie Scattering by Scott Prah, [http://omlc.org/calc/mie\\_calc.html](http://omlc.org/calc/mie_calc.html), (Accessed May 9, 2018).
- [17] J. Loste, J.M. Lopez-Cuesta, L. Billon, H. Garay, M. Save, Transparent polymer nanocomposites: an overview on their synthesis and advanced properties, *Prog. Polym. Sci.* 89 (2019) 133–158, <https://doi.org/10.1016/j.progpolymsci.2018.10.003>.